Dynamics of nonspherical capsules in shear flow

Prosenjit Bagchi* and R. Murthy Kalluri
Department of Mechanical & Aerospace Engineering, Rutgers, The State University of New Jersey, Piscataway, New Jersey 08854, USA
(Received 15 April 2009; published 10 July 2009)

Three-dimensional numerical simulations using a front-tracking method are presented on the dynamics of oblate shape capsules in linear shear flow by considering a broad range of viscosity contrast (ratio of internal-to-external fluid viscosity), shear rate (or capillary number), and aspect ratio. We focus specifically on the coupling between the shape deformation and orientation dynamics of capsules, and show how this coupling influences the transition from the tank-treading to tumbling motion. At low capillary numbers, three distinct modes of motion are identified: a swinging or oscillatory (OS) mode at a low viscosity contrast in which the inclination angle $\theta(t)$ oscillates but always remains positive; a vacillating-breathing (VB) mode at a moderate viscosity contrast in which $\theta(t)$ periodically becomes positive and negative, but a full tumbling does not occur; and a pure tumbling mode (TU) at a higher viscosity contrast. At higher capillary numbers, three types of transient motions occur, in addition to the OS and TU modes, during which the capsule switches from one mode to the other as (i) VB to OS, (ii) TU to VB to OS, and (iii) TU to VB. Phase diagrams showing various regimes of capsule dynamics are presented. For all modes of motion (OS, VB, and TU), a large-amplitude oscillation in capsule shape and a strong coupling between the shape deformation and orientation dynamics are observed. It is shown that the coupling between the shape deformation and orientation is the strongest in the VB mode, and hence at a moderate viscosity contrast, for which the amplitude of shape deformation reaches its maximum. The numerical results are compared with the theories of Keller and Skalak, and Skotheim and Secomb. Significant departures from the two theories are discussed and related to the strong coupling between the shape deformation, inclination, and transition dynamics.

DOI: 10.1103/PhysRevE.80.016307 PACS number(s): 47.63.−b, 47.61.Jd, 87.16.D−, 47.57.−s

I. INTRODUCTION

Erythrocytes or red blood cells constitute the major particulate component of blood. The structural composition of these cells is a sac of hemoglobin enclosed by a lipid bilayer and a two-dimensional (2D) network of spectrin filaments [1,2]. This structure gives the cell an extreme flexibility, a unique characteristic which, in a major way, determines the dynamics and rheology of blood. Modeling of the whole cell on the molecular level is, however, prohibitive if interaction among multiple cells is considered or the long-time dynamics of individual cell is of interest. Continuum approaches then become useful by modeling the cells as capsules or vesicles which are viscous liquid drops surrounded by deformable membranes. Typically four quantities determine the mechanical behavior of such deformable particles: the viscosity contrast, the shear and extensional moduli of the membrane, and the bending resistance. Unlike a capsule, a vesicle does not have the shear resistance; rather it has the bending resistance, and its surface area is incompressible.

Erythrocytes, or their simplified models, capsules, and vesicles, exhibit complex dynamics when subject to a shear flow. Early [3,4] and recent [5–10] experiments show primarily two types of motion, a tank-treading motion in which the particle inclines at a steady angle with the flow direction while the interior liquid and the membrane make a continuous rotation and a tumbling motion (TU) in which the particle flips similar to a rigid body. The tank-treading and tumbling motions of a particle in a shear flow $\mathbf{u}=\{\dot{\gamma}y,0,0\}$ can be predicted analytically by the Keller-Skalak (KS) theory [11]. In the KS theory, the particle is assumed to be a shape-preserving ellipsoid of semimajor and minor axes lengths L and B, and is composed of an inextensible membrane and an internal fluid of viscosity $\lambda\mu_o$, and immersed in a fluid of viscosity μ_o (Fig. 1). The KS theory predicts that the time-dependent inclination angle $\theta(t)$ between the major axis and the flow direction is given by

$$\dot{\theta}=-\frac{\dot{\gamma}}{2}-\frac{2LB}{L^2+B^2}\dot{\phi}+\frac{\dot{\gamma}}{2}\frac{L^2-B^2}{L^2+B^2}\cos 2\theta, \tag{1}$$

where $\dot{\gamma}$ is the shear rate and $\dot{\phi}$ is the tank-treading frequency given by

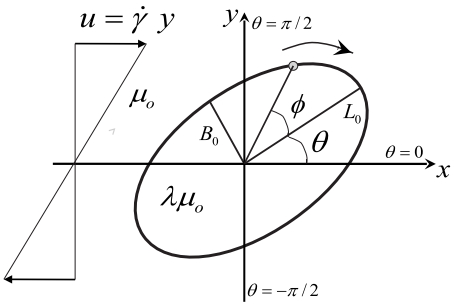

FIG. 1. Schematic showing a capsule in shear flow. Here θ is the inclination angle of the major axis with the flow direction (x) and ϕ is the phase angle of a surface Lagrangian point. $0<\theta<\pi/2$ is the extensional quadrant and $-\pi/2<\theta<0$ is the compressional quadrant of the shear flow $\mathbf{u}=\{\dot{\gamma}y,0,0\}$.

*Corresponding author; pbagchi@jove.rutgers.edu

 ©2009 The American Physical Society

$$\dot{\phi} = -\frac{\dot{\gamma} f_3}{f_2 - \lambda f_1} \cos 2\theta, \tag{2}$$

where f_1, f_2, and f_3 are dimensionless, and they depend on the axes ratios [11,12]. For a given geometry, the tank-treading motion is predicted when the viscosity contrast λ is less than a critical value λ_c, and the tumbling motion is predicted when $\lambda > \lambda_c$. In the tumbling mode, $\dot{\phi} = 0$.

The major limitations, among others, of the KS theory are that it assumes a shape-preserving particle and that the results are independent of the shear rate. Erythrocytes, capsules, and vesicles can undergo a large-amplitude shape deformation in shear flow [3–10]. Analytical theories exist for capsules and vesicles in the limit of small deformation [13–15]. Numerical simulations are required when large deformation is considered which have successfully predicted the tank-treading and tumbling motions of capsules [16–19] and vesicles [20–25].

Recent experiments have suggested the existence of a swinging or oscillatory (OS) motion of red blood cells [5], nonspherical capsules [6], and vesicles [7,8], in addition to the tank-treading and tumbling modes. Numerical simulations have also predicted swinging of capsules [18,19] and vesicles [25]. Experiments [5] and simulations [18] have shown that the transition from tank treading to tumbling of erythrocytes and capsules can be triggered by decreasing the shear rate while the viscosity contrast remains constant, thus departing from the KS theory. The oscillatory dynamics and the shear-dependent transition are recently addressed theoretically by Skotheim and Secomb (SS) [12] within the framework of the KS theory. Introducing the elastic energy of the membrane as $E = E_o \sin^2 \phi$, an additional term $f_3 \dot{\gamma} U_e \sin 2\phi / (f_2 - \lambda f_1)$ was included in the right-hand side (rhs) of Eq. (2) where $U_e = E_o / V \mu_o \dot{\gamma} f_3$, and V is the volume of the particle. Though the SS model can predict the shear-rate-dependent transition from tank treading to tumbling, it neglects a large deformation in shape. Experiments on viscous vesicles have shown that the shape deformation plays a very significant role in the inclination and transition dynamics [9,10]. A vacillating-breathing (VB) mode of vesicles has been observed experimentally [8–10] and predicted analytically [14,15,26,27] and numerically [24,25]. This mode appears in the vicinity of $\lambda = \lambda_c$ and is characterized by the vesicle swinging about its mean inclination angle $\theta_o \approx 0$ accompanied by a large-amplitude shape deformation.

It appears, therefore, that the shape deformation plays a major role in the inclination and transition dynamics of vesicles and capsules, and most likely for erythrocytes, despite the differences in their mechanical characteristics [28]. Both the KS and SS theories neglect the influence of deformability. Experiments have shown that even in the pure tumbling mode, the shape deformation makes $\theta(t)$ deviate from that predicted by the KS theory [9]. Understanding the influence of shape deformation on the transition dynamics of capsules and vesicles is receiving a growing interest in recent years using state-of-the-art experimental [7–10] and computational [18–25,29] approaches, and higher-order analytical theories [14,15,26,27,30,31].

The objectives of this paper are (i) to further improve our understanding of the coupling between the shape deformation and orientation dynamics and (ii) to show how this coupling influences the transition from tank-treading to tumbling motion and leads to significant departures from the KS and SS theories. The emphasis is on how the dynamics changes, with increasing viscosity contrast, from the oscillating to vacillating-breathing to tumbling motions when large shape deformation is considered. We focus exclusively on the dynamics of capsules with initially oblate shapes. Using three-dimensional numerical simulations of capsules in large deformation, we present results over a broad range of the parameters, namely, (i) viscosity contrast, (ii) shear rate, and (iii) aspect ratio.

II. METHODOLOGY

We consider an initially oblate capsule suspended in a linear shear flow (Fig. 1). The liquids exterior and interior of the capsule are incompressible and Newtonian. The viscosities are μ_o and $\lambda \mu_o$, respectively, where λ is the viscosity contrast. The semimajor and minor axes of the undeformed capsule in the plane of shear are L_o and B_o, respectively. The constitutive law governing the capsule membrane is described by a strain energy function W due to Skalak *et al.* [32] as

$$W = \frac{E_s}{12}[I_1^2 + 2(I_1 - I_2)] + \frac{E_a}{12} I_2^2, \tag{3}$$

where $I_1 = \epsilon_1^2 + \epsilon_2^2 - 2$ and $I_2 = \epsilon_1^2 \epsilon_2^2 - 1$ are the surface strain invariants, ϵ_1 and ϵ_2 are the principal extension ratios, and E_s and E_a are the shear elasticity and area dilatation moduli, respectively. The first term in the rhs of Eq. (3) represents the shear resistance of the membrane, while the second term represents the resistance against area dilatation. The membrane is nearly incompressible when $E_a \gg E_s$. Bending resistance of the membrane is not considered. Since deformation of the capsule occurs, the semimajor and minor axes lengths vary with time and are denoted by $L(t)$ and $B(t)$. The half axis length in the vorticity direction is $Z(t)$. The Taylor deformation parameter, a dimensionless measure of capsule deformation, is defined as $D = (L - B)/(L + B)$.

In our earlier publications [33,34], we have described the numerical method in a greater detail. In brief, we have developed a front-tracking code for capsule deformation in three dimensions, following the technique developed for drop deformation [35] that is originally based on the immersed boundary method [36,37]. In this method, the entire flow field that includes both the internal and external liquids is discretized using a fixed (Eulerian) mesh, and the capsule surface is discretized using a moving (Lagrangian) mesh. Invoking an indicator function $I(\mathbf{x},t)$, which is unity for the internal fluid and zero for the external fluid, the viscosity in the entire flow field can be written as

$$\mu(\mathbf{x},t) = \mu_0[1 + (\lambda - 1) I(\mathbf{x},t)]. \tag{4}$$

The fluid motion is governed by the continuity and Navier-Stokes equations as

$$\nabla \cdot \mathbf{u} = 0, \tag{5}$$

$$\rho\left[\frac{\partial \mathbf{u}}{\partial t} + \mathbf{u} \cdot \nabla \mathbf{u}\right] = -\nabla p + \nabla \cdot \mu[\nabla \mathbf{u} + (\nabla \mathbf{u})^T], \tag{6}$$

where $\mathbf{u}(\mathbf{x},t)$ is the fluid velocity, ρ is the density, and p is the pressure. The fluid/structure coupling is done by adding a body force $\mathbf{F}(\mathbf{x},t)$ to the rhs of Eq. (6) which is related to the elastic force $\mathbf{f}(\mathbf{x}',t)$ generated in the capsule membrane as

$$\mathbf{F}(\mathbf{x},t) = \int_S \mathbf{f}(\mathbf{x}',t)\delta(\mathbf{x}-\mathbf{x}')d\mathbf{x}', \tag{7}$$

where $\mathbf{x}$ is the Eulerian grid, $\mathbf{x}'$ is a Lagrangian point on the cell surface, S is the capsule surface, and δ is the three-dimensional Delta function. The Navier-Stokes equations are solved to obtain the velocity and pressure fields in the entire flow domain. The no-slip condition on the capsule surface is imposed by extracting the surface velocity from the surrounding fluid as

$$\mathbf{u}_S(\mathbf{x}',t) = \int_\Omega \mathbf{u}(\mathbf{x},t)\delta(\mathbf{x}-\mathbf{x}')d\mathbf{x}, \tag{8}$$

where Ω implies the flow domain. The Lagrangian points on the membrane are then advected as

$$\frac{d\mathbf{x}'}{dt} = \mathbf{u}_S(\mathbf{x}',t). \tag{9}$$

The viscosity $\mu(\mathbf{x},t)$ is updated by solving a Poisson equation for the indicator function $I(\mathbf{x},t)$ as

$$\nabla^2 I = \nabla \cdot \mathbf{G}, \tag{10}$$

where $\mathbf{G}=\int_S \delta(\mathbf{x}-\mathbf{x}')\mathbf{n}d\mathbf{x}'$ and $\mathbf{n}$ is the unit vector normal to the capsule surface. For numerical implementation, a smooth representation of the δ function is used, which spans over four Eulerian grids [35]. A combined second-order finite difference scheme and Fourier transform is used for the spatial discretization, and a second-order time-split scheme is used for the temporal discretization of the Navier-Stokes equations. The computation domain is a cube having lengths 2π times the capsule radius. The Eulerian resolution used here is 80^3. The capsule surface is discretized using 5120 triangular elements (Fig. 4). A Lagrangian node on the surface is surrounded by five or six triangular elements. The elastic forces acting on the three vertices of a triangular element are obtained from the strain energy function W using the principal of virtual work as $\mathbf{f}(\mathbf{x}',t)=-\partial W/\partial \mathbf{x}'$. The detailed method of computing $\mathbf{f}(\mathbf{x}',t)$ on a triangulated surface is given in [33,34,38,39]. In brief, the problem is first reduced to a 2D (planar) deformation by transforming the undeformed and deformed surface elements to a common plane using rigid-body rotations. This gives the in-plane displacements $\mathbf{v}$ of the vertices and the displacement gradient tensor $\mathbf{D}$. The in-plane stretch ratios become

$$\epsilon_i^2 = \frac{1}{2}[G_{11}+G_{22} \pm \sqrt{\{(G_{11}-G_{22})^2+4G_{12}^2\}}], \quad i=1,2, \tag{11}$$

where $\mathbf{G}=\mathbf{D}^{\mathrm{T}}\mathbf{D}$. Then, the in-plane force $\mathbf{f}^P$ can be obtained as

$$\mathbf{f}^P = \frac{\partial W}{\partial \epsilon_1}\frac{\partial \epsilon_1}{\partial \mathbf{v}} + \frac{\partial W}{\partial \epsilon_2}\frac{\partial \epsilon_2}{\partial \mathbf{v}}. \tag{12}$$

In our earlier publications [33,34], detailed validations of the methodology for capsule deformation in shear flow have been presented. We observed that a spherical capsule deforms into a steady ellipsoidal shape at a constant inclination angle with the flow direction. Comparisons were presented with respect to (w.r.t.) the experimental results [6], small deformation theory [13], and boundary-integral simulations [16,17]. Hence we do not repeat the validation in the present paper. Note that the choice of the front-tracking method, as opposed to the boundary-integral method, is due to the straightforward implementation and versatility of the former. A comparison of the numerical efficiency of the two methods is beyond the scope of this work.

The major dimensionless parameters are (i) the capillary number $\mathrm{Ca}=\mu_o a\dot{\gamma}/E_s$, where a is the radius of a spherical capsule with the same volume of the initially oblate capsule, (ii) the viscosity contrast λ, and (iii) the aspect ratio $\alpha = B_o/L_o$. The ratio $C=E_a/E_s$ is fixed at unity. Thus the area incompressibility condition is not satisfied. We vary Ca from 0.02 to 0.4, λ from unity to 25, and α between 0.6 and 0.9. The effect of inertia is neglected. Below, all lengths are scaled by a. The dimensionless time is denoted by $t^*=t\dot{\gamma}$.

III. RESULTS

We begin with the description of the capsule dynamics at "low shear" ($\mathrm{Ca}\leq 0.1$ typically) at $\mathrm{Ca}=0.05$. Figure 2 shows the time-dependent inclination angle $\theta(t)$, deformation parameter D, and semimajor (L) and semiminor (B) axes. Here we describe the transition in the capsule dynamics that is observed in the simulations as the viscosity contrast λ is increased. We show the results for three viscosity contrasts, $\lambda=3$, 7, and 10, all for an aspect ratio of $\alpha=0.7$.

For the $\lambda=3$ case in Fig. 2(a), the numerical results show that the inclination angle $\theta(t)$ does not remain constant, rather it oscillates with time. Here $\theta(t)$ is always positive $[0<\theta(t)<\pi/2]$ and it varies periodically between $\theta_{\max}$ and $\theta_{\min}$. The capsule shape is also not stationary, and the angular oscillation is accompanied by a periodic shape deformation as evident from the D, L, and B plots in Fig. 2(a). The lengths of the major and minor axes oscillate with a large amplitude. The oscillatory (or swinging) motion of the capsule is superimposed with a tank-treading motion of the membrane. The tank-treading motion is described in Fig. 3 where the phase angle $\phi(t)$ of a surface Lagrangian point is shown. For the $\lambda=3$ case, $\phi(t)$ decreases smoothly from $\pi/2$ to $-\pi/2$ (and $\dot{\phi}<0$ in accordance with the direction of vorticity of the flow) implying the tank-treading motion of the capsule membrane.

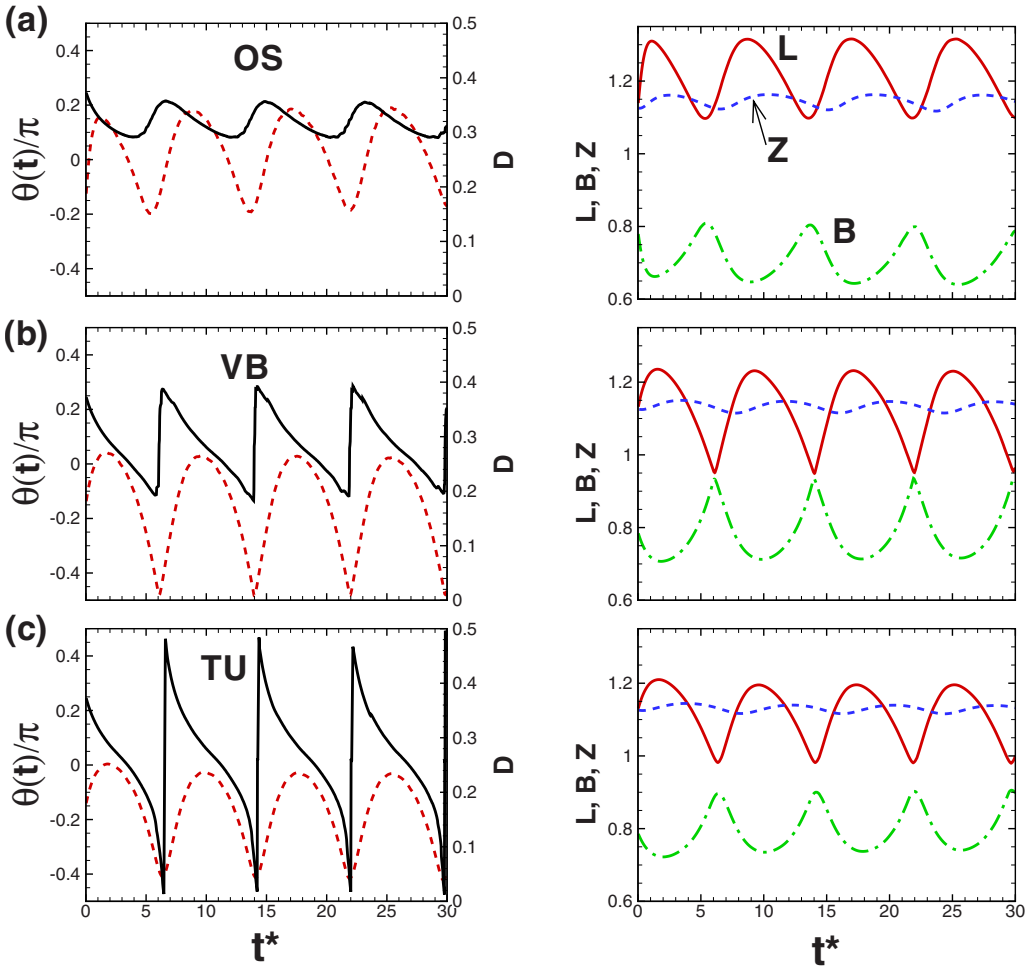

FIG. 2. (Color online) Capsule dynamics at low shear (Ca=0.05) showing OS, VB, and TU motions. Left panel shows the inclination angle $\theta(t)$ (solid black line) and the deformation parameter D (dash red line). Right panel shows the semimajor (L, red solid line) and minor (B, green dashed-dotted line) axes, and the half axis length in the vorticity direction (Z, dash blue line). All lengths are scaled by a and time by $1/\dot{\gamma}$. Note that $(L-B)_{\min}$ and $D_{\min}$ are nearly zero for the VB case shown in (b).

Consider now the $\lambda=10$ case as shown in Fig. 2(c). A tumbling motion is observed here which is indicated by the inclination angle $\theta(t)$ going from $+\pi/2$ to $-\pi/2$. Even for this tumbling case, a significant shape deformation is evident as D, L, and B oscillate with a large amplitude. The phase angle $\phi(t)$ oscillates between its maximum and minimum (Fig. 3) whose magnitude remains less than $\pi/2$, and $\dot{\phi}$ is both positive and negative, implying that a Lagrangian point oscillates back and forth along the capsule surface and that the tank-treading motion is inhibited.

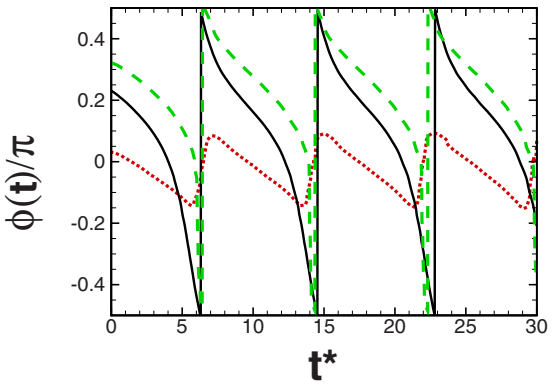

FIG. 3. (Color online) Phase angle $\phi(t)$ for the three cases shown in Fig. 2. $\lambda=3$, black solid line; $\lambda=7$, green dash line; $\lambda=10$, red dotted line.

Consider now an intermediate viscosity contrast at $\lambda=7$ in Fig. 2(b). Here $\theta(t)$ periodically becomes positive and negative but it does not reach $\pm\pi/2$. Hence the capsule does not make a full tumbling. Instead, it makes a large-amplitude swinging motion about a mean inclination which is close to zero. A sharp increase in $\theta(t)$ occurs while going from $\theta_{\min}$ to $\theta_{\max}$ which is associated with a large-amplitude shape oscillation as evident from the D, L, and B plots in Fig. 2(b). Figure 3 shows that for this case the phase angle ϕ ranges in $\pm\pi/2$, and $\dot{\phi}$ is always negative, implying that the tank-treading motion still exists.

The numerical results presented above suggest that the capsule dynamics at the intermediate viscosity contrast ($\lambda=7$ here) is distinct from the oscillatory motion at a lower λ and the tumbling motion at a higher λ. This can be further understood by comparing the amplitude of shape deformation for the three cases. The amplitudes of $D(t)$, $L(t)$, and

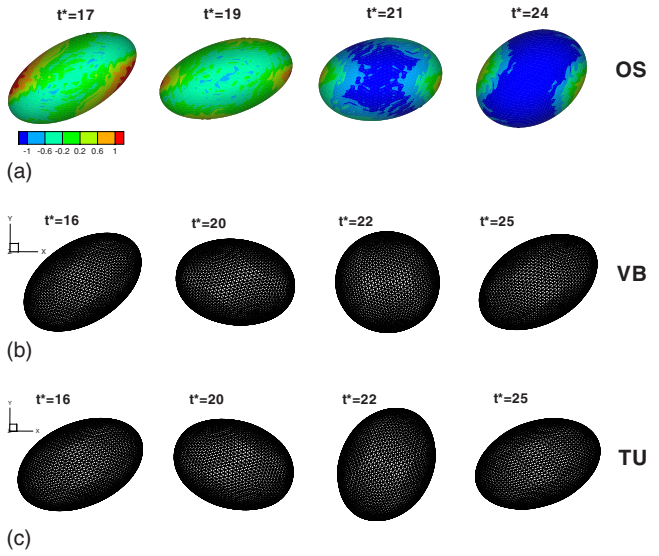

FIG. 4. (Color online) Instantaneous shapes for the OS, VB, and TU motions at Ca=0.05. For all cases, $\alpha=0.7$. From top to bottom, λ varies as 3, 7, and 10 (compared with Fig. 2). For the OS case, we show the contours of the principal tension T_2^P in arbitrary unit. The darker (blue in color) region corresponds to a high compressive stress. The numerical mesh for capsule surface discretization is also shown.

$B(t)$ are higher at $\lambda=7$ than those at $\lambda=3$ and 10. Most interestingly, the minimums of $L-B$ and D, that is, $(L-B)_{\min}$ and $D_{\min}$, first decrease as λ is increased from 3 to 7, but then increase as λ is increased further to 10. At $\lambda=7$, both $(L-B)_{\min}$ and $D_{\min}$ are nearly zero, meaning that the capsule momentarily attains a near-circular shape in the plane of shear. This happens when $\theta(t)$ becomes negative. It is interesting to note that for $\lambda=7$ the inclination angle $\theta(t)$ and the major and minor axes presented here look qualitatively similar to those of a vacillating-breathing vesicle as predicted theoretically in [26] (see Figs. 3 and 4 therein) and observed experimentally in [10].

Figure 4 shows the capsule shapes at different times for the three viscosity contrasts ($\lambda=3,7,10$). Swinging or oscillatory motion for $\lambda=3$ and tumbling motion for $\lambda=10$ are evident here. For the $\lambda=7$ case, the shape becomes nearly circular in the shear plane during $\theta(t)<0$, while it is elongated during $\theta(t)>0$. This clearly shows that for the intermediate viscosity contrast, the capsule undergoes a significant elongation and compression. The shape at $\theta(t)<0$ is not a mirror image of the shape at $\theta(t)>0$. Further, a full tumbling motion does not occur though $\theta(t)$ becomes negative. A qualitative explanation of this dynamics was given in [14] and is applicable here as well. When $\theta(t)>0$, the capsule is in its elongational state for which the hydrodynamic torque is maximum, and it tends to tumble. As $\theta(t)$ becomes negative, compression starts, and the hydrodynamic torque is reduced, preventing the capsule from making a full tumbling motion. At even higher viscosity contrast (e.g., $\lambda=10$ here), the compression is not significant, and a full tumbling is possible.

The numerical results presented in Figs. 2–4 describe the transition in the capsule dynamics at a low Ca as λ is increased. Three types of motion are evident here, which can be characterized using $\theta(t)$ and $(L-B)_{\min}$. (i) At a low λ, a swinging or OS motion occurs in which the major axis always lies in the extensional quadrant of the shear flow, with $0<\theta(t)\leq\pi/4$ and $(L-B)_{\min}>0$. (ii) At higher λ, a pure TU occurs, which is characterized by $\theta(t)$ varying between $\pm\pi/2$, and $(L-B)_{\min}>0$. (iii) At the intermediate viscosity contrast, a VB-type motion occurs, which is characterized by an increased shape deformation, $(L-B)_{\min}\approx 0$, and $\theta(t)$ being periodically positive and negative without a full tumbling motion.

The above results on the capsule dynamics show two significant departures from the KS theory. First, the KS theory predicts either a steady inclination angle (at a low viscosity contrast) or a tumbling motion (at a higher viscosity contrast), unlike the OS and VB modes seen here. Second, and more interestingly, at the intermediate viscosity contrast, the inclination angle $\theta(t)$ periodically becomes positive and negative without a full tumbling, while in the KS theory the tumbling motion starts as soon as $\theta(t)<0$.

The half axis length $Z(t)$ along the vorticity direction is also shown in Fig. 2. For all modes (OS, VB, and TU), $Z(t)$ shows a small amplitude oscillation. For the OS case Z is mostly less than L. For the VB and TU modes, $Z(t)$ can be greater than $L(t)$, and the capsule momentarily attains a prolate shape whose major axis lies along the vorticity direction.

For the deformation parameter D at $t=0$, D_o (≈ 0.1765) can be compared with $D(t)$ to infer if the capsule is in an elongational or compressional state. For the OS case at $\lambda=3$ [Fig. 2(a)], $D(t)$ is mostly greater than D_o, implying that the capsule spends more time in an extensional state. For the VB ($\lambda=7$) and TU ($\lambda=10$) modes, $D(t)$ is mostly less than D_o, and hence the capsule spends a significant time in the compressional state. To elucidate this point further, we plot in Fig. 4(a) the contours of a principal tension on the capsule membrane defined as $T_2^P=(\partial W/\partial\epsilon_2)/\epsilon_1$. Since the area is not conserved, the membrane can be locally under elongation or compression, and accordingly, T_2^P is either positive or negative. Figure 4(a) shows that T_2^P varies over the capsule surface and becomes periodically positive/negative as the capsule oscillates. When $D(t)$ is maximum, $T_2^P>0$ over most of the surface. When $D(t)<D_o$, a compressional stress develops over a large area around the equatorial region of the capsule. Surprisingly, the compressional stress exists even when the inclination angle $\theta(t)$ is positive. Thus the part of the capsule may be under compression even when its major axis is oriented along the extensional direction of the flow. For all modes (OS, VB, and TU) the maximum magnitude of the compressive stress exceeds that of the extensional stress. We also see (not shown in the figure) that stress magnitude decreases with increasing λ. Further, for low Ca, the compressive stress leads to the onset of buckling in which the capsule membrane folds. Since T_2^P goes periodically positive and negative, we observe that the capsule goes through repeated membrane folding and recovery stages when $D(t)<D_o$ and $D(t)>D_o$, respectively.

The angular orientation and shape deformation are strongly coupled to each other. This coupling has a major influence on the capsule dynamics during the transition from swinging to tumbling mode. We now explore the coupling between the orientation dynamics and the shape deformation

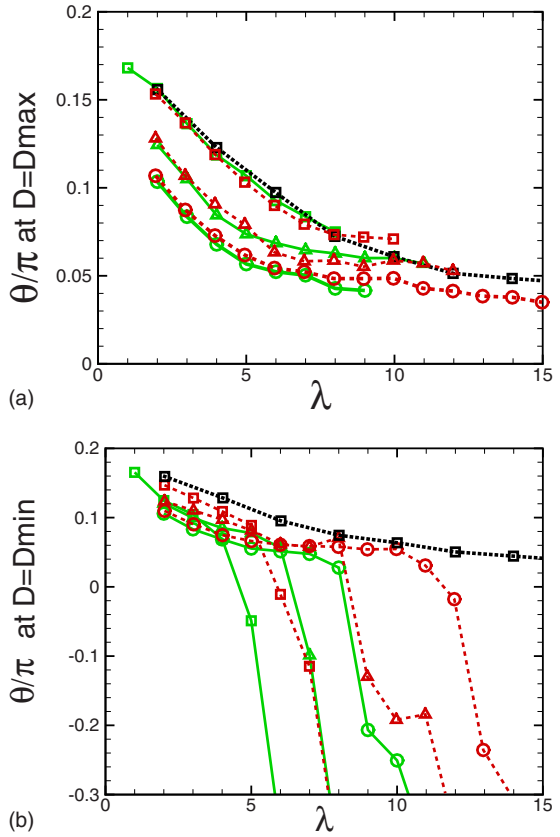

FIG. 5. (Color online) (a) Inclination angle $\theta(t)$ at which D is maximum and (b) $\theta(t)$ at which D is minimum as a function of the viscosity contrast λ for different values of α and Ca. Here α=0.6 (solid green line), 0.7 (dash red line), and 0.9 (dotted black line). Symbols represent Ca=0.05 (squares), 0.1 (delta), and 0.2 (circles).

in more detail. Figure 5(a) shows the inclination angle at which the maximum elongation occurs. We see that the angle at which the capsule elongation reaches its maximum is less than the extensional direction of the flow ($\pi/4$). This angle decreases with increasing Ca (and hence increasing shear). With respect to λ, the angle first decreases rapidly during the OS and VB modes but becomes nearly independent of λ in the TU mode. Further, this angle is independent of α. At low Ca and low λ, the shape relaxation is fast compared to the flow time, and the elongation is in phase with the shear flow. At high Ca and high λ, the relaxation is slow, and the elongation continues for $\theta(t)<\pi/4$. Figure 5(b) shows the inclination angle at which $D(t)$ reaches its minimum. In the OS mode, this angle is positive. With increasing λ the angle decreases rapidly as the transition to VB and TU modes occur. In the VB mode, minimum D occurs for $-\pi/4<\theta<0$. In the TU mode, the compression continues beyond $-\pi/4$ due to slower relaxation, and the minimum D occurs near $\theta=-\pi/2$.

We now show that the shape deformation is maximum for the intermediate λ values when the VB modes occur. For this, we consider the amplitude ΔD of the deformation parameter in Fig. 6. We also examine the value of $(L-B)_{\min}$ (not shown). Several interesting results are noted here which further elucidate the role of shape deformation on the emergence of the VB modes. (i) For a given Ca and α, the amplitude ΔD first increases but then decreases, and $(L-B)_{\min}$ first decreases to nearly zero but then slightly increases with increasing λ. The maximum of ΔD occurs at an intermediate λ for which the VB-type motion occurs so that the capsule momentarily attains a circular shape in the shear plane leading to $(L-B)_{\min}\approx 0$. (ii) ΔD and hence, shape oscillation, increases with decreasing Ca and α. (iii) The viscosity ratio at which ΔD reaches its maximum increases with increasing Ca and α, implying that the VB-type mode onsets at a lower λ for lower shear rates and α. Note that a clear increase in $(L-B)_{\min}$ in the TU regime is observed for Ca$<$0.1. For higher Ca, such an increase is not significant for the range of λ considered here as a significant deformation occurs in the TU regime.

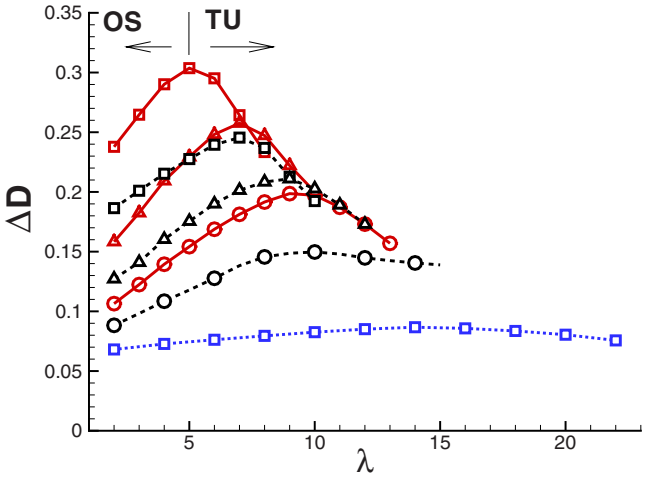

FIG. 6. (Color online) Amplitude of shape deformation ΔD as a function of the viscosity contrast λ for different values of α and Ca. Symbols are as follows: —□—α=0.6, Ca=0.05; —△—α=0.6, Ca=0.1; —○—α=0.6, Ca=0.2; - -□- - α=0.7, Ca=0.05; - -△- - α=0.7, Ca=0.1; - -○- - α=0.7, Ca=0.2; ···□··· α=0.9, Ca=0.05.

Now we present results showing the role of shape deformation in causing departures from the KS and SS models. The time-average inclination angle θ_o is shown in Fig. 7(a) and compared with the KS theory. Both the numerical results and the KS theory show a decrease in θ_o with increasing λ. The agreement between the theory and the numerical results is better for weakly deformable capsules (low Ca) but poor for more deformable capsules (higher Ca). A significant difference between the theoretical and the numerical results occurs in the VB and TU modes, and hence, at higher λ. In the KS theory, the transition from the tank treading to tumbling occurs when $\theta_o=0$ via a saddle-node bifurcation; θ_o decreases faster as λ approaches λ_c. In contrast, the numerical results show a very slow decrease in θ_o near the transition. In the simulations, tumbling occurs even for $\theta_o>0$. Such a slow decrease in θ_o has been reported earlier for vesicles with viscous membranes in [24] using stochastic simulations. Our results show that a qualitatively similar trend occurs for capsules as well and can be predicted by deterministic simulations. This slow decrease in θ_o is due to a nonharmonic variation in θ w.r.t. time arising from the large-amplitude shape deformation and is discussed later.

Figure 7(b) shows the variation in θ_o with Ca and compares the results with the SS theory in the OS regime. Note

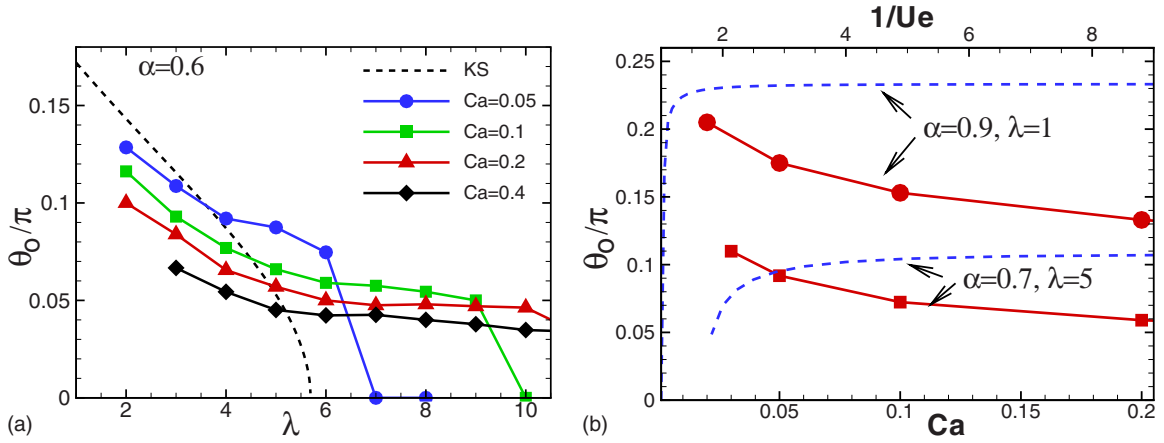

FIG. 7. (Color online) (a) Average inclination angle θ_o as a function of λ for (a) α=0.6. Symbols and/or solid lines are the numerical results. The dash line is the KS theory. (b) Variation in θ_o with respect to Ca. Symbols and solid lines are the numerical results. Dash lines are based on the SS theory.

that in the SS theory, the effect of shear rate is considered via $1/U_e$ which is proportional to but not equal to Ca. Thus a qualitative comparison can be obtained between the theory and the numerical results by choosing a range of values of $1/U_e$. The numerical results show that in the OS regime, θ_o decreases with increasing Ca (or $\dot{\gamma}$). In contrast, the SS theory predicts that θ_o is nearly insensitive to $\dot{\gamma}$ in the OS regime. This discrepancy is because the SS theory neglects the large deformation of capsules which is important at high $\dot{\gamma}$. More elongated shapes that occur at an increasing $\dot{\gamma}$ lead to a reduced θ_o. The decrease in θ_o with increasing Ca has been observed earlier in experiments [6] and numerical simulations [16,17] for spherical capsules, and is in qualitative agreement with the present results for nonspherical capsules.

One important effect of the shape deformation on the orientation dynamics is a nonharmonic variation in the inclination angle $\theta(t)$ with time which results in an "asymmetry" about its time-average value θ_o. The asymmetry in $\theta(t)$, in turn, leads to nonzero values of θ_o, even in the TU regime [Figs. 7(a) and 7(b)], thus departing from the KS theory. We now quantify the asymmetry in $\theta(t)$ as follows. For an OS mode, $\theta(t)$ is always positive, and the asymmetry in $\theta(t)$ can be defined by the ratio τ_2/τ_1 where τ_1 is the time taken by the capsule to go from $\theta_{\min}$ to $\theta_{\max}$, and τ_2 is the time to go from $\theta_{\max}$ to $\theta_{\min}$. In the absence of an asymmetry, the ratio τ_2/τ_1 would be unity. The numerical results for τ_2/τ_1 is shown in Fig. 8 as a function of the viscosity contrast λ. In the OS regime, the numerical results show that $\tau_2/\tau_1 > 1$. This apparently implies that the capsule swings faster in the direction opposite to the rotational motion of the flow. This is because the compression occurs over a longer time, while the elongation occurs much rapidly (Fig. 2). As λ increases, the ratio τ_2/τ_1 increases. It then approaches ∞ as the VB mode onsets at higher λ. In the VB and TU regimes, $\theta(t)$ becomes negative. Then τ_1 and τ_2 are computed as the times for which $\theta(t)$ is negative and positive, respectively (see the inset of Fig. 8). The numerical results show that as the capsule transits from the VB-type to TU-type motion with increasing λ, the ratio τ_2/τ_1 decreases from large values and approaches unity at higher λ. The KS theory predicts that τ_2/τ_1 is always unity for a tumbling capsule. The numerical results show that τ_2/τ_1 can be greater than unity in the TU regime. This implies that the capsule spends more time in the extensional quadrant of the shear flow (though the capsule actually may be under compression even in this orientation, Fig. 4).

Another example of the coupling between the shape deformation and orientation dynamics is shown by the amplitude $\Delta\theta$ of the inclination angle as in Fig. 9. The numerical results are compared with the SS theory. Figure 9(a) shows the variation in $\Delta\theta$ with respect to the viscosity contrast λ for a given Ca. As λ increases, $\Delta\theta/\pi$ increases from small values in the OS regime and approaches unity in the TU regime. In this respect, a qualitative agreement between the numerical results and the SS theory is observed. However, the SS theory predicts a sharp jump in $\Delta\theta$ near $\lambda=\lambda_c$, while the numerical results show a much slower increase. The slower increase in $\Delta\theta$ is due to the emergence of the VB modes for

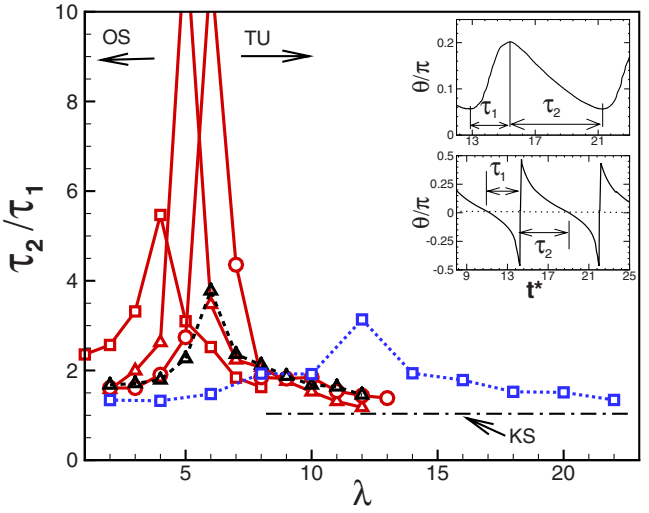

FIG. 8. (Color online) Asymmetry in $\theta(t)$ shown by τ_2/τ_1 as a function of the viscosity contrast λ for different capillary numbers and aspect ratio. Various runs are as follows: —□—α=0.6, Ca =0.05; —△—α=0.6, Ca=0.1; —○—α=0.6, Ca=0.2; - - -△- - - α=0.7, Ca=0.1; - - -□- - - α=0.9, Ca=0.05. Inset shows how τ_1 and τ_2 are obtained from $\theta(t)$ for the OS and TU cases. KS: the Keller-Skalak theory.

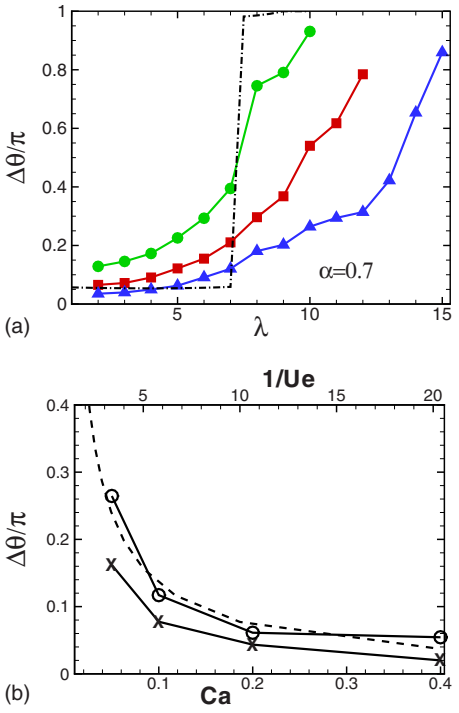

FIG. 9. (Color online) Amplitude of oscillation of the inclination angle w.r.t. (a) λ and (b) Ca. In (a), numerical results are shown by symbols and solid lines (green circle Ca=0.05, red square Ca=0.1, and blue delta Ca=0.2). The dashed-dotted line is the result of the SS model for $1/U_e=5$. All results are for $\alpha=0.7$. In (b) the numerical results are for λ=4 (circle) and λ=2 (x). The dash line is the result for the SS model at λ=4. All results are for $\alpha=0.6$.

which large-amplitude shape deformation occurs which is not considered in the SS model.

Figure 9(b) shows the variation in $\Delta\theta$ with respect to Ca for a given λ. Here we have chosen the data in the OS regime for clarity. The prediction based on the SS theory is also shown by choosing a range of $1/U_e$, for which the numerical data closely follows the theoretical prediction. Similar to the SS theory, the numerical $\Delta\theta$ decreases with increasing Ca (and so $\dot{\gamma}$). So the SS theory can capture the qualitative trend of $\Delta\theta$ with respect to $\dot{\gamma}$ but not with λ.

Figure 10(a) shows the variation in the lengths of the semimajor and minor axes w.r.t. the inclination angle θ for OS, VB, and TU cases. A large variation in the axis lengths is evident here. For all cases, the major axis shows a greater change in its length than the minor axis, that is, $|L_{\max}-L_{\min}|>|B_{\max}-B_{\min}|$. For the OS case, we see that there is a small asymmetry in L and B about the mean inclination angle θ_o. The elongation of the major axis (i.e., when L is increasing) occurs over a smaller variation in θ than its contraction. Similarly, the contraction of the minor axis occurs over a smaller variation in θ than its elongation. This asymmetry implies that the capsule shape at $\theta(t)>\theta_o$ is not a mirror image of that at $\theta(t)<\theta_o$. The asymmetry increases further in the VB mode. When the TU mode is considered for which $\theta_o\approx 0$, we see that L and B are still asymmetric about $\theta_o=0$. The major axis starts to grow, and the minor axis starts to contract when $\theta=\theta_{\max}$ (OS and VB modes) or $\pi/2$ (TU modes). The elongation of the capsule continues for θ

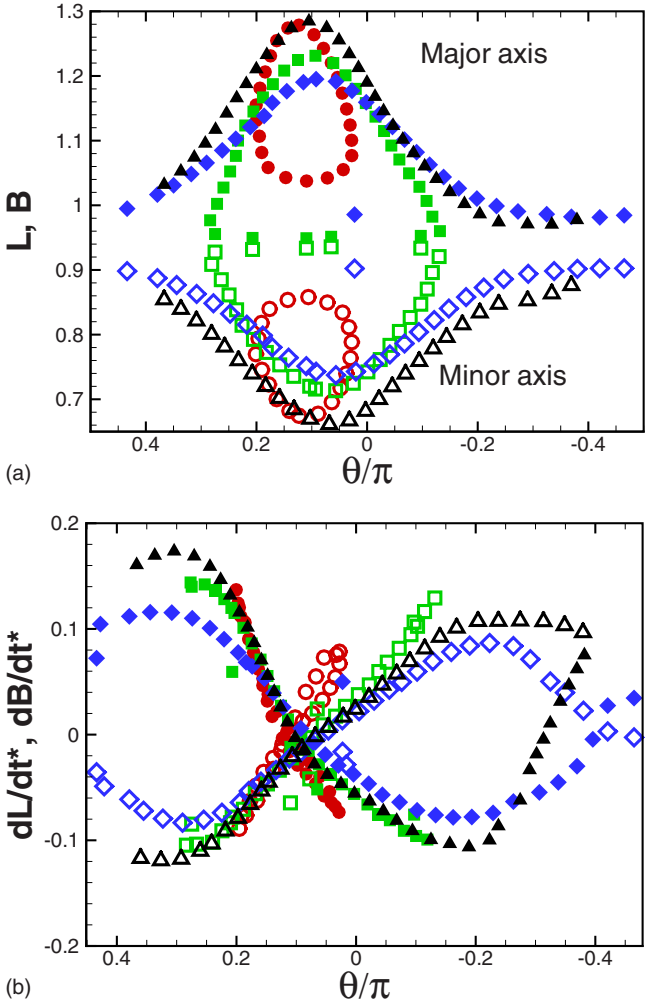

FIG. 10. (Color online) (a) Variation in the semimajor (L, filled symbols) and minor (B, open symbols) axes w.r.t. the inclination angle θ. Symbols are as follows. OS case: red circles ($\alpha=0.7$, Ca=0.05, λ=4). VB case: green squares ($\alpha=0.7$, Ca=0.05, λ=7). TU cases: blue diamond ($\alpha=0.7$, Ca=0.05, λ=10), and black delta ($\alpha=0.6$, Ca=0.05, λ=7). (b) dL/dt (filled symbols) and dB/dt (open symbols) for the similar cases as in (a).

$<\pi/4$. The contraction of the major axis, and elongation of the minor axis, starts even for $\theta>0$ when the capsule is oriented in the extensional quadrant of the flow.

Figure 10(b) shows the rates of elongation and contraction, dL/dt and dB/dt, over θ. For all modes (OS, VB, and TU), the elongation and contraction rates show asymmetry, that is, they are higher when θ is positive than when it is negative. Note that the overall deformation is described by the Taylor parameter D. The results imply that dD/dt is higher when the capsule is aligned with the compressional direction of the shear flow. Thus the elongation of the capsule from a compressional state occurs faster than the other way.

Figure 11 shows the variation in the angular velocity $\dot{\theta}$ with respect to θ. The results for the OS and TU regimes are shown in Figs. 11(a) and 11(b), respectively. In Fig. 11(a) we compare the numerical results ($\dot{\theta}_{\text{num}}$) with the SS theory ($\dot{\theta}_{\text{SS}}$) by choosing a value of $1/U_e$ (but for same λ and α) for

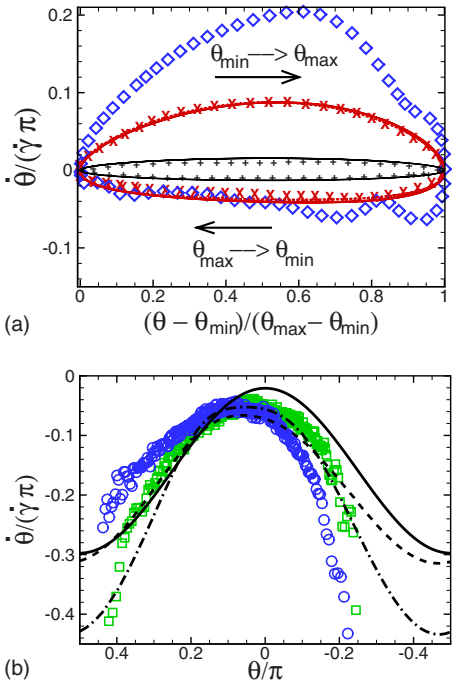

FIG. 11. (Color online) Angular velocity $\dot{\theta}$. (a) Results for OS cases: right and left arrows imply θ going from $\theta_{\min}$ to $\theta_{\max}$, and $\theta_{\max}$ to $\theta_{\min}$, for which $\dot{\theta}$ is positive and negative, respectively. Symbols are numerical results for $\alpha=0.7$ for Ca=0.05, $\lambda=3$ (red X), Ca=0.05, $\lambda=5$ (blue $\diamond$), Ca=0.2, $\lambda=3$ (black +). Lines are the SS theory for $1/U_e=2$, $\lambda=3$ (solid red line), $1/U_e=2$, $\lambda=5$ (dash red line), and $1/U_e=8$, $\lambda=3$ (solid black line). First two SS cases (solid red line and dash red line) nearly overlap in the figure. (b) Results for TU cases. Symbols are numerical results for $\alpha=0.7$ for Ca=0.05, $\lambda=10$ (green squares), and Ca=0.02, $\lambda=5$ (blue circles). Solid black line is the KS theory for $\alpha=0.7$, $\lambda=10$. Dash and dashed-dotted black lines are the SS theory for $\alpha=0.7$ for $1/U_e=1$, $\lambda=10$, and $1/U_e=1.43$, $\lambda=5$, respectively.

which the best agreement is found. The horizontal axis in the plot is $[\theta(t)-\theta_{\min}]/(\theta_{\max}-\theta_{\min})$. In this regime, $\dot{\theta}$ becomes positive and negative due to capsule oscillation. However, $|\dot{\theta}_{\text{num}}|$ is lower when the capsule swings clockwise in the direction of rotation of the flow (i.e., when θ goes from $\theta_{\max}$ to $\theta_{\min}$) than when it goes the other way. This asymmetry is the result of the shape deformation in which elongation occurs faster and over a smaller extent of $\theta(t)$ as discussed before. The magnitude of $\dot{\theta}_{\text{num}}$ in the counterclockwise swing increases rapidly with increasing λ, while that in the clockwise swing increases at a slower rate. The asymmetry also increases with decreasing Ca. The numerical results can be matched with the SS theory by choosing an appropriate value of $1/U_e$. We also noted that the effect of changing Ca can also be matched when we proportionately change U_e, as shown in the figure. However, the effect of changing λ is not predicted correctly by the SS theory which shows that $\dot{\theta}_{\text{SS}}$ is nearly insensitive to changing λ.

Figure 11(b) shows $\dot{\theta}$ for the TU cases and compares the numerical results with the KS and SS theory. Unlike the KS theory for which $\dot{\theta}_{\text{KS}}$ is symmetric about $\theta=0$, the numerical results show a significant asymmetry. Further, $|\dot{\theta}_{\text{num}}|>|\dot{\theta}_{\text{KS}}|$ for $\theta<0$, but $|\dot{\theta}_{\text{num}}|<|\dot{\theta}_{\text{KS}}|$ for $\theta>0$. Hence the numerical tumbling velocity is lower than that predicted by the KS theory when the capsule is in the extensional quadrant of the shear flow. This is because the capsule spends more time in the extensional quadrant as shown earlier ($\tau_2/\tau_1>1$). When the capsule is in the compressional quadrant, the numerical tumbling velocity is higher than that predicted by the KS theory because the capsule spends less time here. When we compare the numerical results with the SS theory, we see that the SS theory can capture the asymmetrical nature of $\dot{\theta}_{\text{num}}$ to some extent, but it still differs from the numerical results.

We now consider the capsule dynamics at "high shear" (Ca$\geq$0.2, typically) as shown in Fig. 12. Here we show time-dependent inclination angle $\theta(t)$, deformation parameter $D(t)$, and the length of the semimajor and minor axes, $L(t)$ and $B(t)$. These simulations are performed for longer times ($t^*>50$). Very interestingly, we see that the same capsule transits from one mode to other over time. For example, in Fig. 12(a) which is for Ca=0.2 and $\lambda=13$, we see that the capsule switches from TU to VB mode at around $t^*\approx 25$ after making one full tumbling motion. In Fig. 12(b) which is for Ca=0.4 and $\lambda=9$, the capsule switches from VB to OS mode at around $t^*\approx 15$. In Fig. 12(c) which is for Ca=0.4 and $\lambda=13$, we see that two transitions occur: from TU to VB at $t^*\approx 20$ and VB to OS at $t^*\approx 30$. We conducted a large number of simulations going up to $\lambda=25$. Based on all simulations, we observe three types of transient states which occur with increasing viscosity contrast as VB$\rightarrow$OS, TU$\rightarrow$VB$\rightarrow$OS, and TU$\rightarrow$VB. The transition is always one way; a transition in the reverse direction is not observed. In agreement with the results in [19], therefore, we do not observe any intermittent dynamics as theoretically predicted by the SS model [12].

Based on our simulation results, we present phase diagrams on λ—Ca plane identifying different dynamical regimes in Fig. 13. At a low Ca, three regimes are observed, namely, OS, VB, and TU, with increasing λ. The VB mode occurs in the neighborhood of $\lambda=\lambda_c$ immediately before transition from the OS to TU modes. Our results show that the VB mode exists over a large range of the viscosity contrast. The critical viscosity contrasts at which OS$\rightarrow$VB and VB$\rightarrow$TU transitions occur increase with increasing Ca and α. The phase diagrams show that the transitions can be triggered below λ_c by decreasing Ca. This behavior is in qualitative agreement with the SS theory and the experiments of Abkarian *et al.* [5] using erythrocytes in shear flow. At higher Ca, the three transient regimes, VB$\rightarrow$OS, TU$\rightarrow$VB$\rightarrow$OS, and TU$\rightarrow$VB, exist in the region between the OS and TU modes. The range of λ over which these transient modes occur increases with increasing Ca. Hence, these transient modes would be important for capsule dynamics at high shear. (Note that the reference to low shear as Ca$\leq$0.1 and high shear as Ca$\geq$0.2 is somewhat arbitrary but motivated by the different dynamics of the capsule seen in the two regimes, i.e., the quasisteady versus the transient modes.)

IV. CONCLUSION

We presented numerical results on the dynamics of oblate shape capsules in shear flow by considering a broad range of

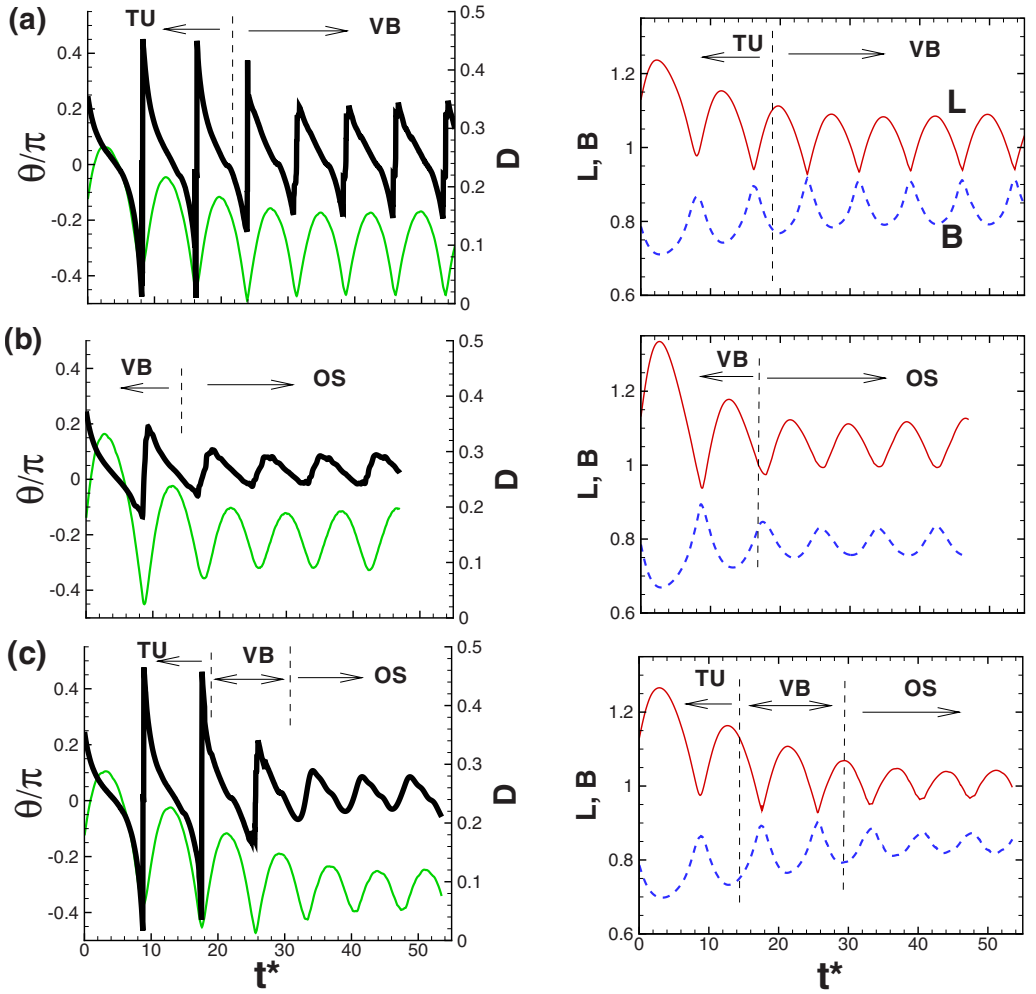

FIG. 12. (Color online) Capsule dynamics at high shear for $\alpha=0.7$. (a) Ca=0.2, $\lambda=13$; (b) Ca=0.4, $\lambda=9$; (c) Ca=0.4, $\lambda=13$. Left panel shows the inclination angle $\theta(t)$ (thick black line) and deformation parameter D (thin green line). Right panel shows semimajor and minor axes lengths, L (solid red line) and B (dash blue line).

viscosity contrast, capillary number, and aspect ratio. The focus of this paper is the coupling between the shape deformation and orientation dynamics, and how this coupling affects the transition dynamics as a function of the viscosity contrast. At low values of Ca, three distinct modes of capsule dynamics are identified. (i) At a low value of λ, a swinging or oscillatory (OS) mode occurs during which the capsule oscillates about a mean inclination angle, but the major axis always lies in the extensional quadrant of the shear flow so that $0<\theta(t)<\pi/4$; the oscillatory motion coexists with the tank treading of the membrane. (ii) At a moderate value of λ, a vacillating-breathing (VB) mode occurs during which the capsule swings vigorously about the mean inclination angle which is close to zero, and $\theta(t)$ periodically becomes positive and negative, but a full tumbling does not occur; a significant compression occurs in this mode leading to the maximum shape deformation. (iii) At even higher values of λ, a pure tumbling mode (TU) occurs; even in this mode, significant shape deformation is observed.

The VB mode of capsules as shown in this paper is qualitatively similar to that for vesicles described in earlier works, e.g., [9,10,14,26–28]. These modes occur because at the intermediate values of λ, the capsule undergoes a significant compression when $\theta(t)$ becomes negative, leading to the near-circular shape, and a reduced hydrodynamic torque. The capsule, as a result, is unable to make a full tumbling motion. Due to the significant compression, the capsule shapes in the extensional and compressional quadrants of the flow are not mirror images about the mean inclination angle. Furthermore, the compression of the capsule occurs at a slower time scale, while the elongation occurs much faster. Thus, in the VB mode, the clockwise swing occurs slower than the counterclockwise swing.

At higher capillary numbers, three types of transient motions occur, in addition to the OS and TU modes, during which the capsule switches from one mode to the other. With increasing λ, these modes appear as (i) VB$\rightarrow$OS, (ii) TU$\rightarrow$VB$\rightarrow$OS, and (iii) TU$\rightarrow$VB.

We analyze the coupling between the shape deformation and orientation dynamics, and we show how this coupling influences the transition from tank-treading to tumbling motion as the viscosity contrast is increased. For all modes of motion (OS, VB, and TU), a large-amplitude oscillation in the capsule shape is observed. The coupling between the shape deformation and orientation is the strongest in the VB mode during which the amplitude of shape deformation ΔD

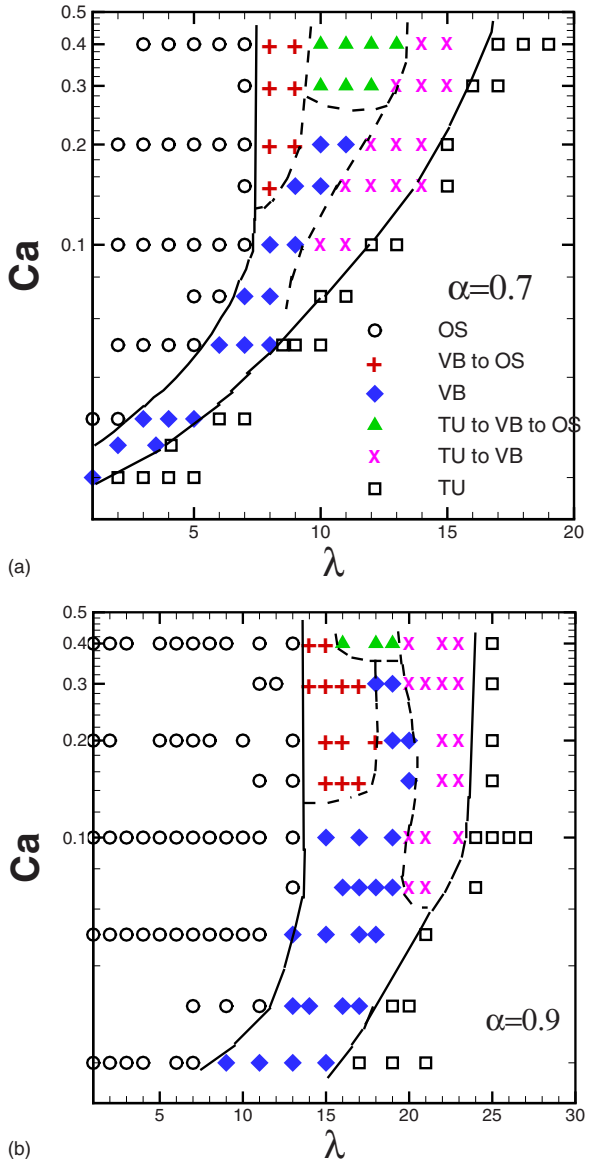

FIG. 13. (Color online) Phase diagrams showing different regimes of capsule dynamics for (a) $\alpha=0.7$ and (b) 0.9.

reaches its maximum, and the capsule shape shows the maximum compression. Hence the shape deformation is most important at an intermediate viscosity contrast around $\lambda=\lambda_c$.

The coupling between the orientation dynamics and the shape deformation leads to a number of significant departures from the KS theory: (i) a steady inclination angle does not exist for $\lambda<\lambda_c$; (ii) as λ approaches λ_c, the inclination angle $\theta(t)$ can become negative without a full tumbling leading to the VB mode; (iii) the inclination angle θ_o is dependent on the shear rate, and it decrease at a much slower rate as λ approaches λ_c, and leads to tumbling even when $\theta_o>0$.

The major departures from the SS theory are (i) the existence of the VB mode at a low Ca for which the shape deformation is the maximum, (ii) the emergence of the transient modes VB→OS, TU→VB→OS, and TU→VB, at higher Ca, and (iii) the absence of any intermittent dynamics. The occurrence of the VB mode cannot be predicted by the SS theory, as this mode corresponds to the maximum shape deformation. Further discrepancies between the SS theory and the numerical results are as follows: (iv) the SS theory predicts that the mean inclination angle θ_o is independent of $\dot{\gamma}$ in the OS regime, but the numerical results show that θ_o decreases with increasing Ca. (v) The large-amplitude oscillation of the inclination angle at the intermediate λ is also not predicted by the SS theory. Unlike in the SS theory, here the shape deformation drives the orientation dynamics at the intermediate viscosity contrasts.

Several other interesting results are presented. The amplitude of shape deformation ΔD first increases reaching its maximum, but then decreases, with increasing λ. The major axis shows a greater variation in length over time than the minor axis. Compression of the capsule occurs at a slower rate than its elongation. Compression starts even when the major axis lies in the extensional quadrant of the flow. Elongation continues for $\theta<\pi/4$; the maximum elongation occurs progressively at an angle lower than $\pi/4$ with increasing λ and Ca. Further, though the capsule spends more time aligned with the extensional direction of the flow, it is actually subjected to a high compressive stress. These results could help in developing a phenomenological model of nonspherical capsule dynamics that can further improve the SS model.

ACKNOWLEDGMENTS

This research is funded by NSF under Grants No. BES-0603035 and No. CTS-0625936. Computational supports from the NSF-funded Teragrid resources at SDSC, TACC, NCSA, and NERSC resources at DOE LBNL are acknowledged.

[1] Q. Zhu, C. Vera, R. J. Asaro, P. Sche, and L. A. Sung, Biophys. J. **93**, 386 (2007).
[2] N. Mohandas and E. Evans, Annu. Rev. Biophys. Biomol. Struct. **23**, 787 (1994).
[3] H. Goldsmith and J. Marlow, Proc. R. Soc. London, Ser. B **182**, 351 (1972).
[4] T. M. Fischer, M. Stohr-Liesen, and H. Schmid-Schonbein, Science **202**, 894 (1978).
[5] M. Abkarian, M. Faivre, and A. Viallat, Phys. Rev. Lett. **98**, 188302 (2007).
[6] H. Rehage, M. Husmann, and A. Walter, Rheol. Acta **41**, 292 (2002).
[7] V. Kantsler and V. Steinberg, Phys. Rev. Lett. **95**, 258101 (2005).
[8] V. Kantsler and V. Steinberg, Phys. Rev. Lett. **96**, 036001 (2006).

[9] M.-A. Mader, V. Vitkova, M. Abkarian, A. Viallat, and T. Podgorski, Eur. Phys. J. E **19**, 389 (2006).
[10] J. Deschamps, V. Kantsler, and V. Steinberg, Phys. Rev. Lett. **102**, 118105 (2009).
[11] S. R. Keller and R. Skalak, J. Fluid Mech. **120**, 27 (1982).
[12] J. M. Skotheim and T. W. Secomb, Phys. Rev. Lett. **98**, 078301 (2007).
[13] D. Barthes-Biesel and J. M. Rallison, J. Fluid Mech. **113**, 251 (1981).
[14] G. Danker, T. Biben, T. Podgorski, C. Verdier, and C. Misbah, Phys. Rev. E **76**, 041905 (2007).
[15] V. V. Lebedev, K. S. Turitsyn, and S. S. Vergeles, New J. Phys. **10**, 043044 (2008).
[16] S. Ramanujan and C. Pozrikidis, J. Fluid Mech. **361**, 117 (1998).
[17] E. Lac, A. Morel, and D. Barthes-Biesel, J. Fluid Mech. **573**, 149 (2007).
[18] Y. Sui, H. T. Low, Y. T. Chew, and P. Roy, Phys. Rev. E **77**, 016310 (2008).
[19] S. Kessler, R. Finken, and U. Seifert, J. Fluid Mech. **605**, 207 (2008).
[20] T. Biben and C. Misbah, Phys. Rev. E **67**, 031908 (2003).
[21] M. Kraus, W. Wintz, U. Seifert, and R. Lipowsky, Phys. Rev. Lett. **77**, 3685 (1996).
[22] J. Beaucourt, F. Rioual, T. Seon, T. Biben, and C. Misbah, Phys. Rev. E **69**, 011906 (2004).
[23] H. Noguchi and G. Gompper, Phys. Rev. Lett. **93**, 258102 (2004).
[24] H. Noguchi and G. Gompper, Phys. Rev. E **72**, 011901 (2005).
[25] H. Noguchi and G. Gompper, Phys. Rev. Lett. **98**, 128103 (2007).
[26] C. Misbah, Phys. Rev. Lett. **96**, 028104 (2006).
[27] P. M. Vlahovska and R. S. Gracia, Phys. Rev. E **75**, 016313 (2007).
[28] M.-A. Mader, H. Ez-Zahraouy, C. Misbah, and T. Podgorski, Eur. Phys. J. E **22**, 275 (2007).
[29] T. Biben, K. Kassner, and C. Misbah, Phys. Rev. E **72**, 041921 (2005).
[30] V. V. Lebedev, K. S. Turitsyn, and S. S. Vergeles, Phys. Rev. Lett. **99**, 218101 (2007).
[31] F. Rioual, T. Biben, and C. Misbah, Phys. Rev. E **69**, 061914 (2004).
[32] R. Skalak, A. Tozeren, P. R. Zarda, and S. Chien, Biophys. J. **13**, 245 (1973).
[33] S. K. Doddi and P. Bagchi, Phys. Rev. E **79**, 046318 (2009).
[34] S. K. Doddi and P. Bagchi, Int. J. Multiphase Flow **34**, 966 (2008).
[35] G. Tryggvason, B. Bunner, A. Esmaeeli, N. Al-Rawahi, W. Tauber, J. Han, S. Nas, and Y. Jan, J. Comput. Phys. **169**, 708 (2001).
[36] C. S. Peskin, J. Comput. Phys. **25**, 220 (1977).
[37] L. A. Miller and C. S. Peskin, J. Exp. Biol. **208**, 195 (2005).
[38] J. M. Charrier, S. Shrivastava, and R. Wu, J. Strain Anal. **24**, 55 (1989).
[39] S. Shrivastava and J. Tang, J. Strain Anal. **28**, 31 (1993).